Pergamon

Acta mater. Vol. 46, No. 14, pp. 5063–5072, 1998

Printed in Great Britain
PII: S1359-6454(98)00162-1
1359-6454/98 $19.00 + 0.00

EFFECTS OF GRAIN BOUNDARIES ON CYCLIC DEFORMATION BEHAVIOR OF COPPER BICRYSTALS AND COLUMNAR CRYSTALS

Z. F. ZHANG† and Z. G. WANG

State Key Laboratory for Fatigue and Fracture of Materials, Institute of Metal Research, Academia Sinica, Shenyang 110015, P.R. China

(Received 5 February 1998; accepted 22 April 1998)

Abstract—In order to reveal the effects of grain boundaries (GBs), the cyclic deformation behavior of a copper columnar crystal containing low-angle GBs, a really grown copper bicrystal RB and a combined bicrystal CB was investigated. The results show that the cyclic stress–strain curve (CSSC) of the copper columnar crystal exhibited a plateau region with saturation resolved shear stress of about 29 MPa over a plastic resolved shear strain range from 6.5×10^{-4} to 4.7×10^{-3}. The electron channeling contrast technique in scanning electron microscopy (SEM-ECC) was applied to observe the cyclically saturated dislocation structures and persistent slip bands (PSBs). In combining the CSSC with the associated saturation dislocation arrangements, it is seen that the strengthening effect of low-angle GBs is very limited. Meanwhile, the CSSC of the combined bicrystal CB was also found to exhibit a plateau region with the saturation resolved shear stress in the range of 29–30 MPa at the plastic resolved shear strain range from 9×10^{-4} to 5.58×10^{-3}. However, the bicrystal RB did not display a plateau in its CSSC, and its saturation stress increased with increasing strain amplitude. Surface observations revealed a GB affected zone (GBAZ) with additional slip near the GB in the bicrystal RB. The width W_{GB} and the volume fraction V_{GB} of the GBAZ increased with increasing strain amplitude. By comparing the CSSCs of the copper bicrystal CB and RB as well as $[\bar{1}35]//[\bar{1}35]$, $[\bar{1}35]//[\bar{2}35]$ and $[\bar{2}35]//[\bar{2}35]$ copper bicrystals, the effects of large-angle and low-angle GBs on cyclic deformation behavior were discussed. A GB strengthening model was proposed by introducing a GB resistance $\Delta\tau_{as}^{B}$ to PSBs and the mean stress σ_{as}^{GB} in the GBAZ. © *1998 Acta Metallurgica Inc. Published by Elsevier Science Ltd. All rights reserved.*

1. INTRODUCTION

It is generally recognized that the flow stress of a polycrystal is greater than that of a single crystal and multiple slip often occurs at the early stage of plastic deformation in a polycrystal due to the presence of grain boundaries (GBs). Each grain in a polycrystal has its own stress–strain characteristic, however, the stress–strain response of the whole polycrystal is not a simple "average" over all the grains. The reason is that the grains do not deform independently owing to the effect of GBs. During the past decades, to clarify the effect of GBs on plastic deformation, different kinds of bicrystals, such as aluminum [1–6], Fe-alloys [7–9] and brass [10–12], have been widely employed. It was found that a GB had a strengthening effect on bicrystals and there was a GB affected zone (GBAZ) in the vicinity of a GB [3–6, 10–14]. The strengthening effect of a GB on a bicrystal was associated with GB properties and component crystal orientations [5, 6]. However, there has been no quantitative expression about the effect of GBs on bicrystals yet. Essentially, GB strengthening is associated with the resistance of the GB to slip bands. However, the GB on a bicrystal did not show a remarkable effect under monotonic plastic deformation conditions [3–6], it is expected that the GB will play a relatively striking role on the bicrystal during cyclic deformation. Meanwhile, GBs in polycrystals are often classified into large-angle and low-angle types. In this paper, the effects of both low-angle and large-angle GBs will be quantitatively discussed on the cyclic deformation behavior by introducing orientation factors (Ω_B and Ω_M) in order to obtain a comprehensive understanding of the cyclic plastic deformation mechanism in a polycrystal.

2. EXPERIMENTAL PROCEDURE

To investigate the effects of large-angle and low-angle GBs on cyclic deformation behavior, two kinds of copper crystals were prepared. Firstly, a columnar crystal containing some low-angle GBs was grown from OFHC copper of 99.999% purity by the Bridgman method in a horizontal furnace. Fatigue specimens containing some low-angle GBs basically parallel to the stress axis were prepared from the as-grown columnar crystal plate, as shown in Fig. 1(a). Secondly, a bicrystal plate of size $200 \times 50 \times 10\ mm^3$ was grown from OFHC copper

†To whom all correspondence should be addressed.

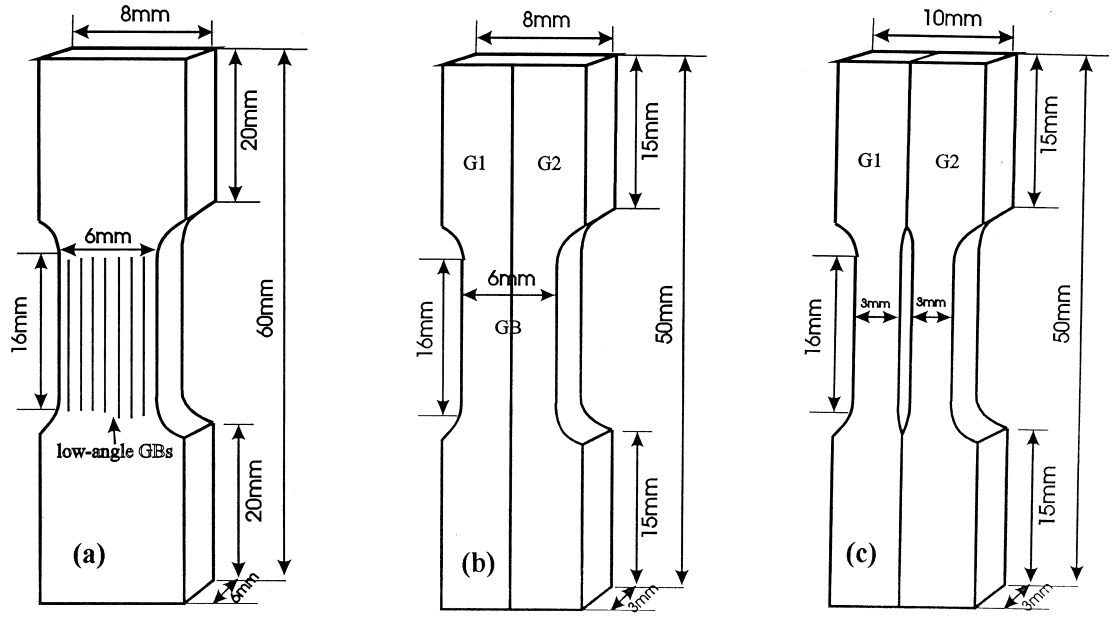

Fig. 1. Fatigue specimens of copper columnar crystal and copper bicrystal RB and CB: (a) the copper columnar crystal; (b) the really grown bicrystal RB; (c) the combined bicrystal CB.

of 99.999% purity by the Bridgman method in a horizontal furnace. The GB in the bicrystal plate is of a large-angle type and along the growing direction. In order to reveal the effect resulting purely from the large-angle GB on cyclic deformation behavior, two kinds of bicrystal fatigue specimens were designed. The fatigue specimen in Fig. 1(b) is made of a really grown bicrystal RB with a GB parallel to the stress axis. The fatigue specimen in Fig. 1(c) is a combined bicrystal CB obtained by sticking two individual single crystals G1 and G2 together at the grip parts, which were separated from the same grown bicrystal plate as the bicrystal RB. Clearly, there is no GB in the gauge portion of the bicrystal specimen CB.

The crystallographic orientations of these specimens were determined by the Laue back reflection technique. The stress axis orientation of the columnar crystal specimen was [$\bar{1}$23] on average. The low-angle GBs in the columnar crystal specimen were closely parallel to the stress axis, and the misorientation between adjacent grains was in the range of about 5°. The stress axis orientations of two component crystals in the bicrystal RB and CB were determined to be G1[$\bar{6}$79] and G2[$\bar{1}$45], respectively. As shown in Fig. 2, all the crystals are oriented for single slip. Before cyclic deformation, all the fatigue specimens were electro-polished carefully for surface observation. Symmetrical push–pull tests were performed on a Shimadzu servo-hydraulic testing machine under strain control at room temperature in air. A triangle wave with a frequency of 0.3 Hz was used. Peak loads in both tension and compression, and hysteresis loops were recorded by computer automatically. After cyclic deformation into saturation, the specimen surfaces were observed by optical microscopy (OM), especially in the vicinity of a GB. Meanwhile, those columnar crystal specimens were polished to observe dislocation patterns within grains and in the vicinity of low-angle GBs or polished and recycled to observe the plastic strain localization by the electron channeling contrast technique in scanning electron microscopy (SEM-ECC) as reported in the literature [15–17].

3. EXPERIMENTAL RESULTS

3.1. Cyclic stress–strain response of the copper columnar crystal

All the columnar crystal specimens exhibited initial cyclic hardening and saturation behavior under the imposed plastic strain amplitudes. The cyclic axial saturation stress varied slightly in the range of 62–63 MPa under the axial plastic strain range from 3.0×10^{-4} to 2.3×10^{-3} as listed in Table 1. The Schmid factor 0.467 of the [$\bar{1}$23] orientation

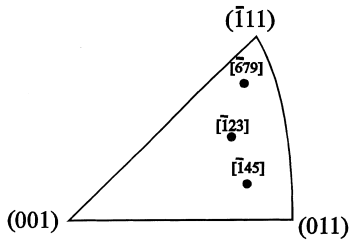

Fig. 2. Crystal orientations in a stereographic triangle in copper columnar crystal and copper bicrystals.

Table 1. The cyclic stress–strain response of the columnar crystal

Specimen No.	T1	T2	T3	T4
ε_{pl} (10^{-3})	0.3	0.8	1.6	2.3
γ_{pl} (10^{-3})	0.65	1.7	3.4	4.7
σ_{as} (MPa)	62.1	62.5	63.0	62.7
τ_{as} (MPa)	29.1	29.3	29.5	29.4

ε_{pl}, axial plastic strain amplitude; γ_{pl}, plastic resolved shear strain amplitude; σ_{as}, axial saturation stress; τ_{as}, saturation resolved shear stress.

was used to calculate the saturation resolved shear stress and plastic resolved shear strain since the misorientation between the adjacent grains was very small (as discussed in the following section). The CSSCs of the copper columnar crystal and the single crystal oriented for single slip [18] are shown in Fig. 3 for comparison. It can be seen that there also exists a plateau region in the CSSC of the copper columnar crystal in the plastic resolved shear strain range from 6.5×10^{-4} to 4.7×10^{-3}. The plateau saturation resolved shear stress was about 29.1–29.5 MPa, basically equal to that (28–30 MPa) of the single-slip-oriented copper monocrystal [18–20].

3.2. Interactions of PSBs and dislocation walls with low-angle GB

The SEM-ECC technique was employed to reveal the interaction of PSBs with low-angle GBs in the columnar crystal. After cyclic saturation, the specimen was electro-polished and recycled. Figure 4(a) and (b) show the plastic strain localization in PSBs and the interaction of PSBs with low-angle GBs. It is consistent with the two-phase model observed in copper single crystals [21, 22]. As the plastic strain amplitude was increased, the volume fraction of PSBs was increased. At a relatively high plastic resolved shear strain amplitude of 4.7×10^{-3}, dislocation wall structures with a channel width of 1.5–1.7 μm were observed, as shown in Fig. 4(c). Moreover, there was no secondary slip in the vicinity of low-angle GBs. As clearly seen in Fig. 4(a)–(c), all the PSBs and dislocation walls can transfer through the low-angle GBs continuously. This result is different from that observed in the vicinity of large-angle GBs where additional slip systems are often activated [3–6, 14].

Large-angle GBs are often considered as an important factor to strengthen polycrystalline materials, and the stress–strain incompatibility at GBs has been discussed extensively [14]. However, the effect of low-angle GBs on cyclic deformation behavior has been seldom reported. From the results above, it is reasonable to conclude that the stress and strain must be compatible at low-angle GBs. The additional resistance of low-angle GBs to PSBs

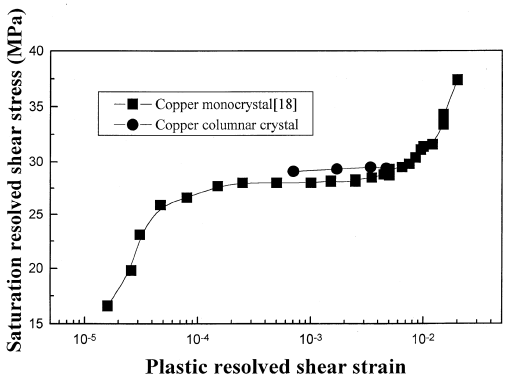

Fig. 3. CSSCs of copper columnar crystal and copper single crystal [18].

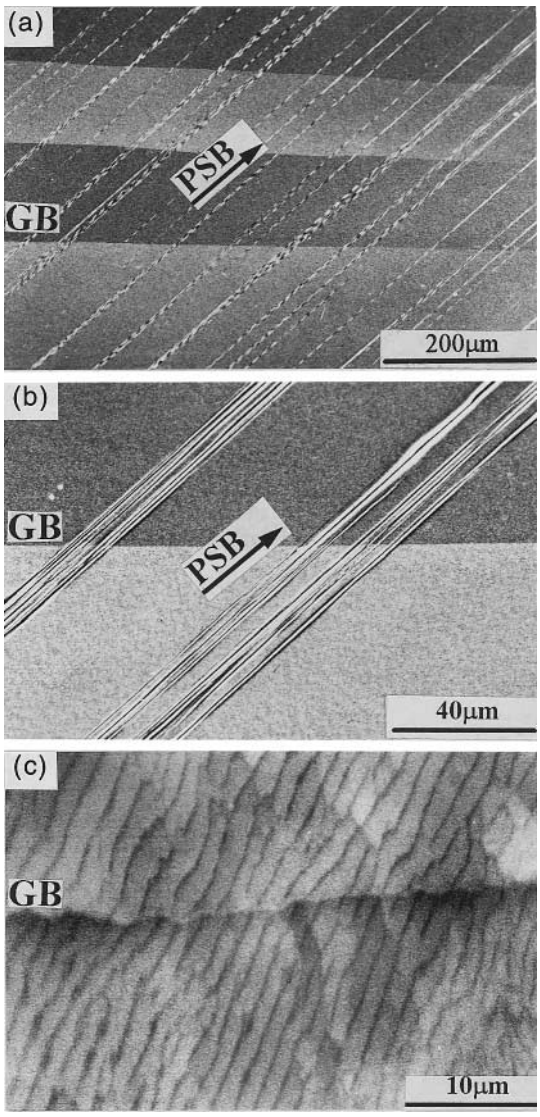

Fig. 4. Plastic strain localization in PSBs and saturation dislocation patterns in the vicinity of low-angle GBs in copper columnar crystal. The copper columnar crystal cycled at plastic resolved shear strain of 1.7×10^{-3} for 10^4 cycles: (a) low magnification; (b) high magnification. The copper columnar crystal cycled at plastic resolved shear strain of 4.7×10^{-3} for 5×10^3 cycles: (c) dislocation walls in the vicinity of low-angle GBs.

Table 2. The cyclic stress–strain responses of the copper bicrystals CB and RB

	ε_a (10^{-3})	ε_{pl} (10^{-3})	σ_{as} (MPa)	γ_{pl} (10^{-3})	τ_{as} (MPa)
CB	1.0	0.36	73.6	0.90	29.4
	1.5	0.84	74.0	2.10	29.6
	2.0	1.34	74.5	3.35	29.8
	2.5	1.82	74.8	4.55	29.9
	3.0	2.23	75.0	5.58	30.0
RB	1.0	0.35	78.5	0.88	31.4
	1.5	0.83	80.2	2.08	32.1
	2.0	1.32	81.8	3.30	32.7
	2.5	1.81	83.5	4.53	33.3
	3.0	2.20	84.8	5.50	34.0

can be negligible. Consequently, the CSSC of the columnar crystal showed a plateau region with the saturation resolved shear stress of 29.1–29.5 MPa similar to the single-slip oriented copper single crystal.

3.3. Cyclic stress–strain responses of copper bicrystal CB and RB

Both bicrystal CB and RB exhibited initial cyclic hardening and saturation behavior at the applied strain amplitudes. Their axial saturation stresses σ_{as} and axial saturation plastic strain amplitudes ε_{pl} at different strain amplitudes are listed in Table 2. The curves of axial saturation stress amplitude vs axial saturation plastic strain amplitude of the bicrystals CB and RB are shown in Fig. 5(a). It can be seen that the CSSC of the combined bicrystal CB showed a plateau region with the axial saturation stress in the range of 73.6–75 MPa at an axial plastic strain range of 3.6×10^{-4}–2.23×10^{-3}. However, the axial saturation stress of the bicrystal RB was obviously higher than that of the combined bicrystal CB and increased with increasing strain amplitude.

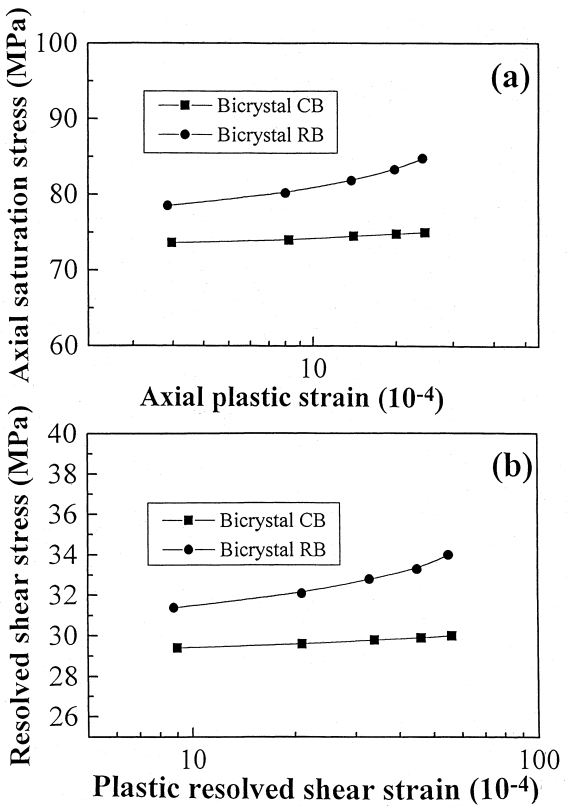

Fig. 5. CSSCs of the combined bicrystal CB and the really grown bicrystal RB: (a) the curves of axial saturation stress vs axial plastic strain; (b) the curves of saturation resolved shear stress vs plastic resolved shear strain.

The saturation resolved shear stresses τ_{as} and the plastic resolved shear strains γ_{pl} of the bicrystal CB and RB can be calculated by introducing an orientation factor ($\Omega_B = 0.40$) of the bicrystal in the following section. For the combined bicrystal CB

$$\tau_{as}^{CB} = \sigma_{as}^{CB}\Omega_B,\ \gamma_{pl}^{CB} = \varepsilon_{pl}^{CB}/\Omega_B. \quad (1)$$

And, for the really grown bicrystal RB

$$\tau_{as}^{RB} = \sigma_{as}^{RB}\Omega_B,\ \gamma_{pl}^{RB} = \varepsilon_{pl}^{RB}/\Omega_B. \quad (2)$$

As shown in Fig. 5(b), the plateau saturation resolved shear stress (29–30 MPa) of the combined bicrystal CB was basically equal to that (28–30 MPa) of the copper single crystal oriented for single slip [18–20]. However, the really grown bicrystal RB exhibited a higher saturation resolved shear stress than the combined bicrystal CB and did not show a plateau region in its CSSC. This difference in saturation stresses is believed to be purely due to the effect of large-angle GB and will be discussed in the following section.

3.4. Surface slip morphology in the bicrystal CB and RB

Surface observations by optical microscopy revealed that only the primary slip system B4 $(111)[\bar{1}01]$ was activated within component crystals (G1,G2) of the combined bicrystal (CB) under all the applied strain amplitudes. It is clear that the cyclic plastic strains of the combined bicrystal CB were carried by the primary slip bands within two component crystals (G1,G2). However, the secondary slip besides the primary slip was observed within the component crystal G2 near the GB in the bicrystal RB, as shown in Fig. 6(a)–(d). The primary slip lines were regularly modulated by the secondary slip lines and no other slip systems were involved. The primary slip lines and secondary slip lines emerged alternately in the GBAZ to form a

cross-weaved structure, which was similar to the deformation bands (DBs) in appearance. This phenomenon should be associated with the serious stress–strain incompatibility at GB. The measured mean width W_{GB} and volume fraction V_{GB} of the secondary slip region are listed in Table 3. It implied that the width W_{GB} and volume fraction V_{GB} of the GBAZ increased and the interaction of primary slip with the secondary slip became more serious with increasing strain amplitude. In general, the macroscopic strain compatibility conditions at a GB plane can be fulfilled if the total number of independently operating slip systems in both neighboring crystals is four [1, 23]. However, it is interesting to note that the total number of activating slip systems is only three beside the GB in the present really bicrystal RB.

4. DISCUSSION

4.1. Orientation factors of copper bicrystal and columnar crystal

The Schmid factor Ω is widely used to calculate the resolved shear stress of single crystals from the imposed axial stress. For polycrystals, the Taylor factor (M = 3.06) or the Sachs factor (M = 2.24) are often employed [24–28]. However, the orientation factor of a bicrystal has seldom been discussed. Hu *et al.* [29, 30] selected the mean value of Schmid factors of two component grains to illustrate the CSSCs of copper bicrystals. But the crystallographic basis for this selection is not clear.

For a bicrystal specimen with two individual grains G1 and G2 combined in parallel, as shown in Figs 1(c) and 7, the two component crystals will deform independently owing to the absence of a GB. As the bicrystal specimen CB was cyclically saturated, according to the force balance

$$P_{as}^{CB} = P_{as}^{G1} + P_{as}^{G2} \tag{3}$$

and

$$\sigma_{as}^{CB} A_{CB} = \sigma_{as}^{G1} A_{G1} + \sigma_{as}^{G2} A_{G2} \tag{4}$$

where P_{as}^{CB}, P_{as}^{G1} and P_{as}^{G2} are the loads applied to the cyclically saturated combined bicrystal CB and the component crystals (G1,G2); σ_{as}^{CB}, σ_{as}^{G1} and σ_{as}^{G2} are the mean axial saturation stresses applied to the bicrystal CB and the component crystals (G1,G2); Ω_B, Ω_{G1}, Ω_{G2} are the orientation factors of the bicrystal CB and the component crystals (G1,G2); A_{CB}, A_{G1} and A_{G2} are the areas of the bicrystal CB and the component crystals (G1,G2); substituting the saturation resolved shear stresses (τ_{as}^{G1}, τ_{as}^{G2} and τ_{as}^{CB}) and Schmid factors (Ω_{G1}, Ω_{G2} and Ω_B) of two component crystals and the combined bicrystal CB gives

$$\frac{\tau_{as}^{CB}}{\Omega_B} A_{CB} = \frac{\tau_{as}^{G1}}{\Omega_{G1}} A_{G1} + \frac{\tau_{as}^{G2}}{\Omega_{G2}} A_{G2}. \tag{5}$$

It is well known that the saturation resolved shear stress τ_{as}^{PSB} of the single copper crystal oriented for single slip maintained a constant value in the range of 28–30 MPa in region B of its CSSC and was independent of crystal orientations [19]. Hence

$$\tau_{as}^{CB} = \tau_{as}^{G1} = \tau_{as}^{G2} = \tau_{as}^{PSB}. \tag{6}$$

Substituting equation (6) into equation (5) gives

$$\frac{1}{\Omega_B} = \frac{V_{G1}}{\Omega_{G1}} + \frac{V_{G2}}{\Omega_{G2}}. \tag{7}$$

Thus, the orientation factor Ω_B of the bicrystal can be described as

$$\Omega_B = \left(\frac{V_{G1}}{\Omega_{G1}} + \frac{V_{G2}}{\Omega_{G2}} \right)^{-1} \tag{8}$$

where V_{G1} and V_{G2} are volume fractions of G1 and G2 in the bicrystal, respectively. It is known that $V_{G1} = V_{G2} = 0.5$, and $\Omega_{G1} = 0.35$, $\Omega_{G2} = 0.47$. Substituting the values of V_{G1}, V_{G2}, Ω_{G1} and Ω_{G2} into equation (8), gives $\Omega_B = 0.40$. Similarly, for the columnar crystal with some low-angle GBs parallel to the stress axis, its orientation factor can be expressed as

$$\Omega_M = \left(\frac{V_{G1}}{\Omega_{G1}} + \frac{V_{G2}}{\Omega_{G2}} + \cdots + \frac{V_{Gn}}{\Omega_{Gn}} \right)^{-1}. \tag{9}$$

For the present copper columnar crystal, its orientation factor should be approximately equal to the Schmid factor of the $[\bar{1}23]$ orientation owing to the small misorientation among the adjacent grains, i.e.

$$\Omega_M = \Omega_{G1} = \Omega_{G2} = \cdots = \Omega_{Gn} = \Omega_{[\bar{1}23]} = 0.467. \tag{10}$$

Essentially, the orientation factors (Ω_B,Ω_M) of the bicrystal and the columnar crystal can be regarded as a geometrical transformation factor, by which the saturation resolved shear stresses along the primary slip direction of the copper bicrystal and the columnar crystal can be calculated.

4.2. Comparison of CSSCs in copper bicrystals

In order to have a better understanding of the effect of GBs on cyclic deformation behavior, the CSSCs of the copper bicrystals CB and RB as well as $[\bar{1}35]/[\bar{1}35]$, $[\bar{1}35]/[\bar{2}35]$ and $[\bar{2}35]/[\bar{2}35]$ copper

Table 3. The width and volume fraction of grain boundary affected zone (GBAZ)

Strain amplitude	0.1%	0.15%	0.2%	0.25%	0.3%
D_{GB} (μm)	265	360	440	540	650
V_{GB} (%)	4.4	6.0	7.3	9.0	10.5

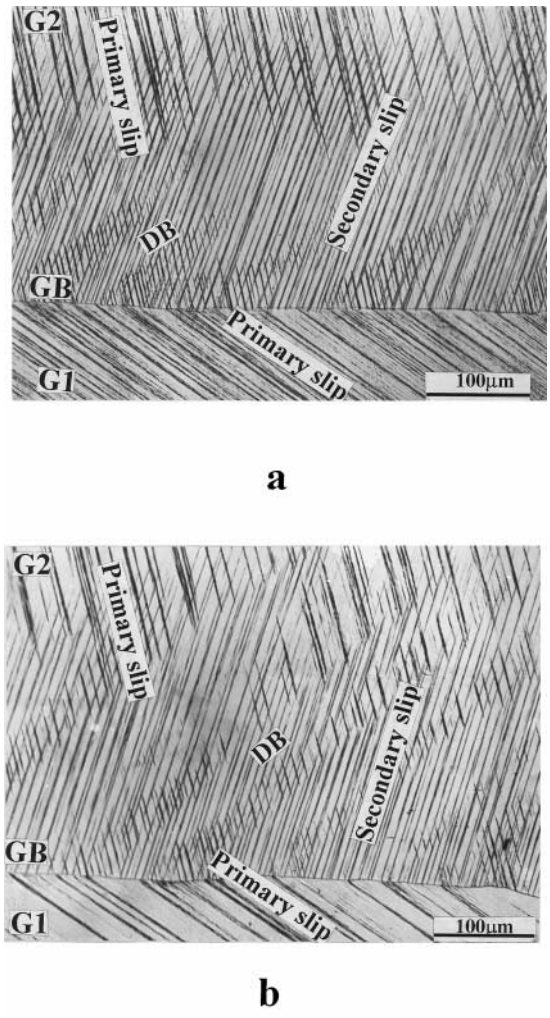

Fig. 6. *Caption opposite.*

bicrystals [29, 30] are shown in Fig. 8. For comparison, the saturation resolved shear stresses were calculated by using the orientation factor Ω_B of the bicrystal. It can be seen that nearly all the CSSCs show a plateau region except the bicrystal RB. But the plateau saturation resolved shear stresses are quite different. For the $[\bar{1}35]/[\bar{1}35]$ bicrystal [29] and the bicrystal CB, their plateau saturation resolved shear stresses are nearly the same, namely 29–30 MPa, and hence basically equal to that (28–30 MPa) of copper single crystals [18–20]. It is indicated that the strengthening effect of the GB in the co-axial $[\bar{1}35]/[\bar{1}35]$ bicrystal can be negligible. For the $[\bar{1}35]/[\bar{2}35]$ and $[\bar{2}35]/[\bar{2}35]$ copper bicrystals [30], their plateau resolved shear stresses (about 32.5 and 36 MPa) are different and higher than that (28–30 MPa) of copper single crystals. It implies that the strengthening effect of a GB can be increased by changing the combination of component crystals and GB properties. However, the saturation resolved shear stress of the bicrystal RB is always higher than that (29–30 MPa) of the bicrystal CB and increased with increasing strain amplitude without showing a plateau region. It can be attributed to the effect of the GBAZ produced by a GB and will be explained as follows.

4.3. Effect of large-angle GB on cyclic saturation stress

The effect of large-angle GB on the flow stresses was extensively discussed for bicrystals with GBs parallel to the stress axis [1–6, 10–14]. Chuang and Margolin [10] have given a stress relation for iso-axial β-brass bicrystals as

$$\sigma_T = \sigma_B + V_{GB}(\sigma_{GB} - \sigma_B) \tag{11}$$

where σ_{GB} was defined as the average stress in GBAZ. It can be determined from the applied stress σ_T, the flow stress σ_B of a single crystal and the volume fraction V_{GB} in GBAZ. The increase in flow stress of the bicrystal is attributed to the existence of GBAZ. Mirura and Saeki [3], and Mirura

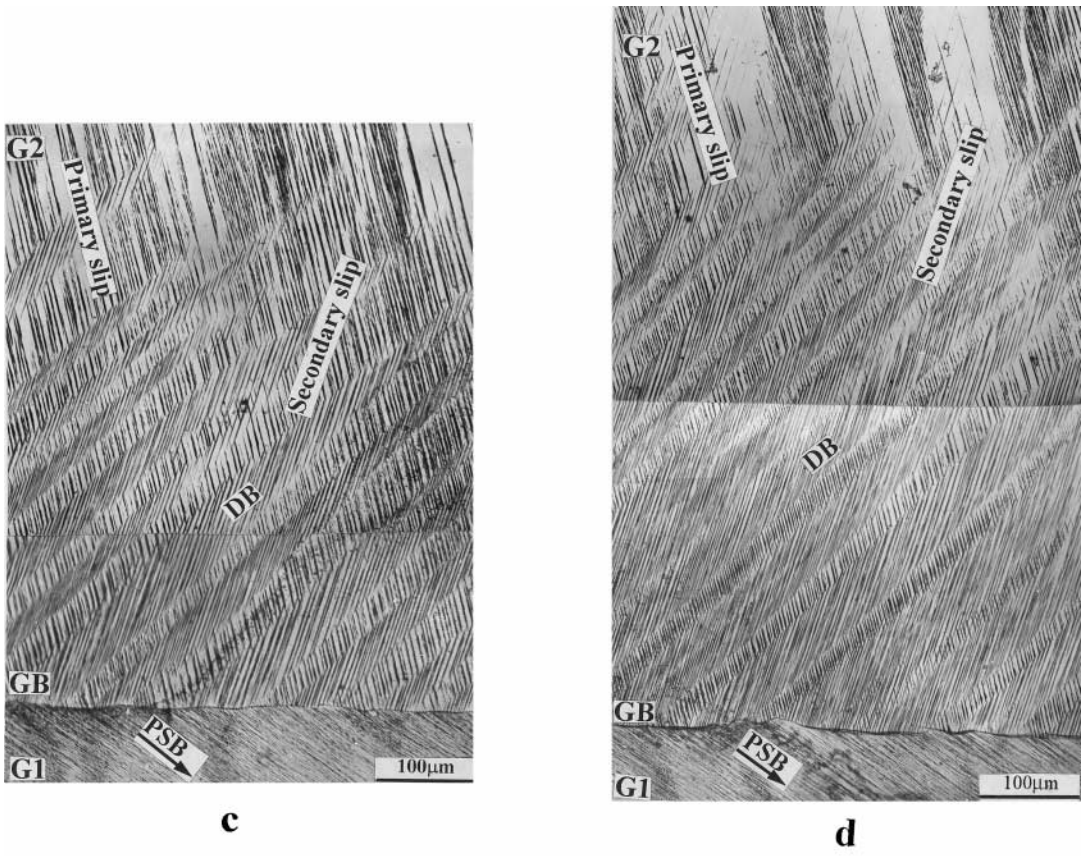

Fig. 6. Slip patterns in the vicinity of GBs in the really grown bicrystal: (a) $\varepsilon_a = 1 \times 10^{-3}$; (b) $\varepsilon_a = 1.5 \times 10^{-3}$; (c) $\varepsilon_a = 2.5 \times 10^{-3}$; (d) $\varepsilon_a = 3 \times 10^{-3}$.

et al. [4] also found that the flow stresses of bicrystals were increased by the presence of Σ7 and Σ21 coincidence GBs.

As shown in Fig. 6(a)–(d), there is a GBAZ in the really grown bicrystal RB subjected to cyclic deformation. However, there is no such GBAZ in the combined bicrystal CB. Apparently, the difference in saturation stresses between the bicrystal CB and RB can be attributed to the higher mean stress in the GBAZ. As the bicrystals (CB and RB) were cyclically saturated, their axial saturation stresses [see Fig. 9(a) and (b)] will have a relation similar to equation (11), i.e.

$$\sigma_{as}^{RB} = \sigma_{as}^{CB} + V_{GB}(\sigma_{as}^{GB} - \sigma_{as}^{CB}) \tag{12}$$

and

$$\sigma_{as}^{CB} = \sigma_{as}^{G1} V_{G1} + \sigma_{as}^{G2} V_{G2} \tag{13}$$

where σ_{as}^{G1}, σ_{as}^{G2}, σ_{as}^{CB}, σ_{as}^{RB}, σ_{as}^{GB} are the axial saturation stresses in the component crystals (G1,G2), the bicrystals (CB,RB) and in the GBAZ, respectively; V_{G1}, V_{G2}, V_{GB} are the volume fractions of the component crystals (G1,G2), and GBAZ. As listed in Table 2, the difference in axial saturation stresses between the bicrystal CB and RB can be simply calculated by the following relation:

$$\Delta\sigma_{as}^{B} = \sigma_{as}^{RB} - \sigma_{as}^{CB}. \tag{14}$$

If $\Delta\sigma_{as}^{GB}$ is attributed to the higher mean stress σ_{as}^{GB} in the GBAZ, by combining equations (12)–(14), σ_{as}^{GB} in the GBAZ can be expressed as

$$\sigma_{as}^{GB} = \frac{\sigma_{as}^{RB} - \sigma_{as}^{CB}}{V_{GB}} + \sigma_{as}^{CB} = \frac{\Delta\sigma_{as}^{B}}{V_{GB}} + \sigma_{as}^{CB}. \tag{15}$$

The calculated results of $\Delta\sigma_{as}^{B}$ and σ_{as}^{GB} at different strain amplitudes are listed in Table 4. It can be

Table 4. The stresses in the GBAZ

Strain amplitude	0.1%	0.15%	0.2%	0.25%	0.3%
$\Delta\sigma_{as}^{B}$ (MPa)	4.9	6.2	7.3	8.7	9.8
σ_{as}^{GB} (MPa)	184.6	177.3	174.1	171.5	168.5
$\Delta\tau_{as}^{B}$ (MPa)	1.96	2.48	2.92	3.48	3.92

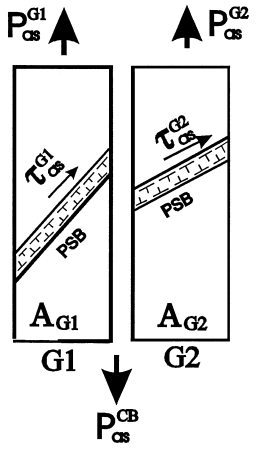

Fig. 7. Diagrammatic sketch of stress distribution in a combined bicrystal CB.

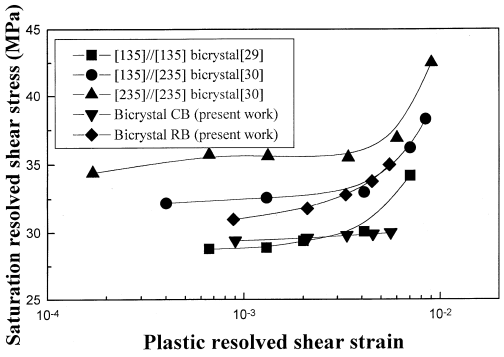

Fig. 8. CSSCs of the bicrystal RB and CB as well as the [$\bar{1}$35]//[1$\bar{3}$5], [$\bar{1}$35]//[$\bar{2}$35] and [$\bar{2}$35]//[$\bar{2}$35] copper bicrystals.

seen that the mean stress σ_{as}^{GB} in the GBAZ is much higher than the mean stresses (σ_{as}^{CB},σ_{as}^{RB}) of the combined bicrystal CB and the really bicrystal RB, and decreases with increasing strain amplitude. It is generally recognized that the stress σ_{as}^{GB} in the GBAZ is not a constant value and decreases apart from GB [10, 12]. Actually, the mean stress σ_{as}^{GB} in the GBAZ can be expressed more precisely as

$$\sigma_{as}^{GB} = \sigma_{as}^{CB} + \frac{\int_0^{V_{GB}} \Delta\sigma_{as}^{B}(V)\,\mathrm{d}V}{V_{GB}} \tag{16}$$

where $\Delta\sigma_{as}^{B}(V)$ is a function of the position and decreases apart from the GB, as shown in Fig. 9(b). Thus, it may be responsible for the reduction of the higher mean stress σ_{as}^{GB} in the GBAZ.

From the viewpoint of plastic strain localization, the cyclic plastic strain of the bicrystal is carried by PSBs within the component crystals G1 and G2 according to the two-phase model [21, 22]. As shown in Fig. 10(a) and by using equations (1) and (6), the saturation resolved shear stress of the bicrystal CB can be described as

$$\tau_{as}^{CB} = \tau_{as}^{PSB} = \sigma_{as}^{CB}\left(\frac{V_{G1}}{\Omega_{G1}} + \frac{V_{G2}}{\Omega_{G2}}\right)^{-1}. \tag{17}$$

When PSBs meet a GB, an additional shear stress should be applied to PSBs due to the constraint of GB, as shown in Fig. 10(b). Consequently, the bicrystal RB would have a higher saturation stress than the bicrystal CB owing to the effect of GB. The saturation resolved shear stress τ_{as}^{RB} of the bicrystal RB can be calculated from equation (2) as

$$\tau_{as}^{RB} = \sigma_{as}^{RB}\left(\frac{V_{G1}}{\Omega_{G1}} + \frac{V_{G2}}{\Omega_{G2}}\right)^{-1}. \tag{18}$$

Combining equations (17) and (18), the additional GB resistance $\Delta\tau_{as}^{B}$ to PSBs can be introduced as

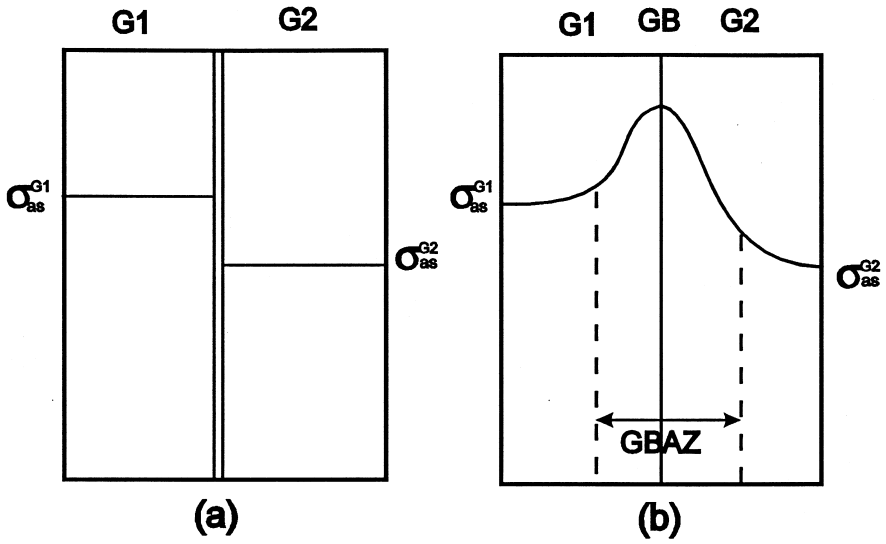

Fig. 9. Diagrammatic sketch of axial saturation stress distribution in the combined bicrystal CB and the really grown bicrystal RB: (a) the combined bicrystal CB; (b) the really grown bicrystal RB.

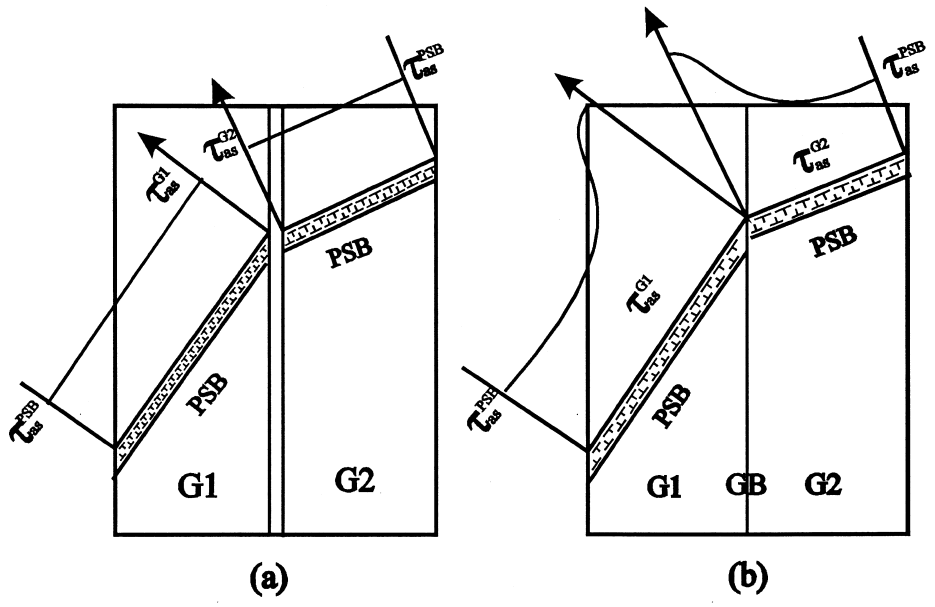

Fig. 10. Diagrammatic sketch of saturation resolved shear stress distribution in the combined bicrystal CB and the really grown bicrystal RB: (a) the combined bicrystal CB; (b) the really grown bicrystal RB.

$$\Delta\tau_{as}^{B} = \tau_{as}^{RB} - \tau_{as}^{PSB} = (\sigma_{as}^{RB} - \sigma_{as}^{CB})\left(\frac{V_{G1}}{\Omega_{G1}} + \frac{V_{G2}}{\Omega_{G2}}\right)^{-1}. \quad (19)$$

The calculated additional GB resistances $\Delta\tau_{as}^{B}$ at different strain amplitudes are listed in Table 4. It can be seen that the additional GB resistance $\Delta\tau_{as}^{B}$ also increases with increasing strain amplitude. For the analysis and calculations above, it seems that the existence of a GBAZ with a higher stress may be responsible for the increase of the cyclic saturation stress and the disappearance of the plateau region in the CSSC of the really grown bicrystal RB.

5. CONCLUSIONS

Cyclic deformation behavior of the copper columnar crystal containing low-angle GBs and the copper bicrystals (CB,RB) was investigated and compared with that of $[\bar{1}35]//[\bar{1}35]$, $[\bar{1}35]//[\bar{2}35]$ and $[\bar{2}35]//[\bar{2}35]$ copper bicrystals. The following conclusions can be drawn.

1. The copper columnar crystal containing low-angle GBs showed a plateau region with saturation resolved shear stress of about 29.1–29.5 MPa in its CSSC at plastic resolved shear strain range from 6.5×10^{-4} to 4.7×10^{-3}. With the SEM-ECC technique, it was found that the stress and strain in the vicinity of low-angle GBs should be compatible. By combining its CSSC with saturation dislocation arrangement, it was suggested that the strengthening effect of low-angle GBs is very limited.
2. The CSSC of the combined bicrystals CB exhibited a plateau region with a saturation resolved shear stress of about 29.4–30.0 MPa. However, the cyclic saturation stress of the really grown bicrystal RB was obviously higher than that of the combined bicrystal CB and increased with increasing strain amplitude without showing a plateau region. The surface observations revealed a GBAZ in the bicrystal RB and the width W_{GB} and volume fraction V_{GB} of GBAZ increased with increasing strain amplitude. By comparing the cyclic saturation stresses between the copper bicrystal CB and RB, a GB strengthening model was proposed by introducing an orientation factor Ω_B, the mean stress σ_{as}^{GB} in the GBAZ and an additional GB resistance $\Delta\tau_{as}^{B}$ to PSBs.

Acknowledgements—This work was financially supported by the National Natural Science Foundation of China (NSFC). The authors are grateful for this support.

REFERENCES

1. Hauser, J. J. and Chalmers, B., *Acta metall.*, 1961, **9**, 802.
2. Davis, K. G., Teghtsoonian, E. and Lu, A., *Acta metall.*, 1966, **14**, 1677.
3. Miura, S. and Saeki, Y., *Acta metall.*, 1978, **26**, 93.
4. Miura, S., Hamashima, K. and Aust, K. T., *Acta metall.*, 1980, **28**, 1591.
5. Rey, C. and Zaoui, A., *Acta metall.*, 1980, **28**, 687.
6. Rey, C. and Zaoui, A., *Acta metall.*, 1982, **30**, 523.
7. Paidar, V., Pal-val, P. P. and Kadeckova, S., *Acta metall.*, 1986, **34**, 2277.
8. Sittner, P. and Paidar, V., *Acta metall.*, 1989, **37**, 1717.
9. Paidar, V., Gemperlova, J. and Pal-val, P. P., *Mater. Sci. Engng*, 1991, **A137**, 69.

10. Chuang, Y.-D. and Margolin, H., *Metall. Trans.*, 1973, **4A**, 1905.
11. Lee, T. D. and Margolin, H., *Metall. Trans.*, 1977, **8A**, P145.
12. Lee, T. D. and Margolin, H., *Metall. Trans.*, 1977, **8A**, 157.
13. Wei, C., Lin, S., Qian, R. G. and Hsiao, J. M., *Acta metall. mater.*, 1991, **39**, 2051.
14. Hirth, J. P., *Metall. Trans.*, 1972, **3A**, 3047.
15. Zauter, R., Petry, F., Bayerlein, M., Sommer, C., Christ, H.-J. and Mughrabi, H., *Phil. Mag.*, 1992, **66**, 425.
16. Schwab, A., Bretchneider, J., Buque, C., Blochwitz, C. and Holste, C., *Phil. Mag. Lett.*, 1996, **74**, 449.
17. Bretschneider, J., Holste, C. and Tippelt, B., *Acta mater.*, 1997, **45**, 3775.
18. Mughrabi, H., *Mater. Sci. Engng*, 1978, **33**, 207.
19. Cheng, A. S. and Laird, C., *Mater. Sci. Engng*, 1981, **51**, 111.
20. Basinski, Z. S. and Basinski, S. J., *Prog. Mater. Sci.*, 1992, **36**, 89.
21. Finney, J. M. and Laird, C., *Phil. Mag.*, 1975, **31A**, 339.
22. Winter, A. T., *Phil. Mag.*, 1974, **30**, 719.
23. Kocks, U. F., *Phil. Mag.*, 1964, **9**, 187.
24. Rasmussen, K. V. and Pedersen, O. B., *Acta metall.*, 1980, **28**, 1467.
25. Pedersen, O. B. and Rasmussen, K. V., *Acta metall.*, 1982, **30**, 1467.
26. Mughrabi, H., *Scripta metall.*, 1979, **13**, 479.
27. Lukas, P. and Kunz, L., *Mater. Sci. Engng*, 1994, **A189**, 1.
28. Wang, Z. R. and Laird, C., *Mater. Sci. Engng*, 1988, **100**, 57.
29. Hu, Y. M., Wang, Z. G. and Li, G. Y., *Scripta mater.*, 1996, **34**, 331.
30. Hu, Y. M., Wang, Z. G. and Li, G. Y., *Mater. Sci. Engng*, 1996, **A208**, 260.